J|A|C|S
ARTICLES
Published on Web 02/18/2006

Proton Permeation into Single Vesicles Occurs via a Sequential Two-Step Mechanism and Is Heterogeneous

Christopher L. Kuyper, Jason S. Kuo, Sarah A. Mutch, and Daniel T. Chiu*

Contribution from the Department of Chemistry, University of Washington, Seattle, Washington 98195-1700

Received October 27, 2005; E-mail: chiu@chem.washington.edu

Abstract: This article describes the first single-vesicle study of proton permeability across the lipid membrane of small (~100 nm) uni- and multilamellar vesicles, which were composed of 1-palmitoyl-2-oleoyl-*sn*-glycero-3-phosphocholine (POPC). To follow proton permeation into the internal volume of each vesicle, we encapsulated carboxyfluorescein, a pH-sensitive dye whose fluorescence was quenched in the presence of excess protons. A microfluidic platform was used for easy exchange of high- and low-pH solutions, and fluorescence quenching of single vesicles was detected with single-molecule total internal reflection fluorescence (TIRF) microscopy. Upon solution exchange and acidification of the extravesicular solution (from pH 9 to 3.5), we observed for each vesicle a biphasic decay in fluorescence. Through single-vesicle analysis, we found that rate constants for the first decay followed a Poisson distribution, whereas rate constants for the second decay followed a normal distribution. We propose that proton permeation into each vesicle first arose from formation of transient pores and then transitioned into the second decay phase, which occurred by the solubility−diffusion mechanism. Furthermore, for the bulk population of vesicles, the decay rate constant and vesicle intensity (dependent on size) correlated to give an average permeability coefficient; however, for individual vesicles, we found little correlation, which suggested that proton permeability among single vesicles was heterogeneous in our experiments.

Introduction

Controlling the permeability of protons across lipid membranes is central to many biological processes, ranging from oxidative phosphorylation in the production of energy for cellular function to the uptake of neurotransmitters into synaptic vesicles that affect neurotransmission. To study proton permeability, synthetic lipid vesicles have proven to be a convenient model system. Several methods for analyzing bulk vesicle measurements have been used to obtain the proton permeability coefficient, which ranges from 10^{-1} to 10^{-9} cm/s.[1−9] This wide variation in rates has been attributed to several factors, including the composition of the lipid bilayer, the temperature, and the method used to calculate the permeability coefficient.[10] Bulk studies have produced a wealth of information and understanding about proton permeability across membranes, yet many questions still remain. We believe that single-vesicle analysis offers information at a finer level of detail and will provide new insights into this biologically important process.

The study and use of individual synthetic lipid vesicles has gained prominence in recent years,[11−15] because of their biomimetic character and the ease of making them on size scales ranging from tens to hundreds of nanometers.[16−18] The properties of individual lipid vesicles vary widely and can be affected by a number of factors, such as the local pH and ionic strength, the concentration of the encapsulated molecules, and the surface characteristics of the vesicle interior. In addition, the rate at which molecules move across lipid membranes is highly dependent on the chemical and physical properties of the membrane, the number of lamellae present in the vesicle, and the ability of the molecule to transport across the lipid bilayer. For instance, small ions exhibit permeability coefficients greater than 10^{-8} cm/s, but water exhibits permeability coefficients of $\sim 10^{-3}$ cm/s.[10]

Characterizing the chemical and physical environments at the single-vesicle level presents an interesting analytical challenge

(1) Nichols, J. W.; Deamer, D. W. *Proc. Natl. Acad. Sci. U.S.A.* **1980**, *77*, 2038.
(2) Nichols, J. W.; Hill, M. W.; Bangham, A. D.; Deamer, D. W. *Biochim. Biophys. Acta* **1980**, *596*, 393.
(3) Cafiso, D. S.; Hubbell, W. L. *Biophys. J.* **1983**, *44*, 49.
(4) Deamer, D. W. *J. Bioenerg. Biomembr.* **1987**, *19*, 457.
(5) Gutknecht, J. *Proc. Natl. Acad. Sci. U.S.A.* **1987**, *84*, 6443.
(6) Nagle, J. F. *J. Bioenerg. Biomembr.* **1987**, *19*, 413.
(7) Norris, F. A.; Powell, G. L. *Biochim. Biophys. Acta* **1990**, *1030*, 165.
(8) Perkins, W. R.; Cafiso, D. S. *Biochemistry* **1986**, *25*, 2270.
(9) Zeng, J.; Smith, K. E.; Chong, P. L.-G. *Biophys. J.* **1993**, *65*, 1404.
(10) Paula, S.; Deamer, D. W. In *Current Topics in Membranes*; Deamer, D. W., Kleinzeller, A., Fambrough, D. M., Eds.; Academic Press: Burlington, MA, 1999; Vol. 48, p 77.
(11) Anderson, B. B.; Chen, G.; Gutman, D. A.; Ewing, A. G. *J. Neurosci. Methods* **1999**, *88*, 153.
(12) Chiu, D. T.; Wilson, C. F.; Ryttsén, F.; Strömberg, A.; Farre, C.; Karlsson, A.; Nordholm, S.; Gaggar, A.; Modi, B. P.; Moscho, A.; Garza-López, R. A.; Orwar, O.; Zare, R. N. *Science* **1999**, *283*, 1892.
(13) Boukobza, E.; Sonnenfeld, A.; Haran, G. *J. Phys. Chem. B* **2001**, *105*, 12165.
(14) Okumus, B.; Wilson, T. J.; Lilley, D. M. J.; Ha, T. *Biophys. J.* **2004**, *87*, 2798.
(15) Karlsson, A.; Sott, K.; Markström, M.; Davidson, M.; Konkoli, Z.; Orwar, O. *J. Phys. Chem. B* **2005**, *109*, 1609.
(16) Hope, M. J.; Bally, M. B.; Webb, G.; Cullis, P. R. *Biochim. Biophys. Acta* **1985**, *812*, 55.
(17) Mayer, L. D.; Hope, M. J.; Cullis, P. R. *Biochim. Biophys. Acta* **1986**, *858*, 161.
(18) Szoka, F.; Olson, F.; Heath, T.; Vail, W.; Mayhew, E.; Papahadjopoulos, D. *Biochim. Biophys. Acta* **1980**, *601*, 559.

considering the very small volumes (10^{-18}−10^{-21} L) and the number of molecules encapsulated inside. To date, the most common approach has been based on fluorescence microscopy, owing to its ability to detect single molecules with high spatial (hundreds of nanometers) and temporal (hundreds of nanoseconds) resolution. Such fluorescence-based single-vesicle studies have yielded interesting observations that are inaccessible to bulk measurements. For example, Zare and co-workers monitored the enzyme activity of very small numbers of alkaline phosphatase molecules within single vesicles and observed temporal fluctuations in the rate of enzymatic turnover.[19] Ha and co-workers encapsulated single ribozyme molecules within 100−200-nm-diameter vesicles and found heterogeneity among single ribozymes to be intrinsic and not caused by interactions with the membrane surface.[14] For single vesicles, very few or even single molecules can be readily encapsulated;[13] yet, for applications such as drug delivery, encapsulation efficiencies become an important parameter. Recently, Sun and Chiu measured the encapsulation efficiency of individual vesicles and observed the efficiency to vary widely between large (>1-μm-diameter) vesicles, depending on the lamellarity, morphology, and size of the vesicle.[20]

This article presents the first single-vesicle study of proton permeability across the membranes of small (∼100 nm) uni- and multilamellar vesicles. To measure the proton flux into the small intravesicular volume, we encapsulated carboxyfluorescein, a pH-sensitive dye,[21,22] inside the vesicle and monitored the quenching rate of dye fluorescence. We used a microfluidic platform for easy solution exchange, a clean surface to induce adsorption of the vesicles onto the glass coverslip (which formed the floor of the channel), and single-molecule total internal reflection fluorescence (TIRF) microscopy to measure the quenching of dye fluorescence. Upon solution exchange through the microchannel and acidification of the extravesicular solution, we observed for each vesicle a biphasic decay in carboxyfluorescein fluorescence. Using the intrinsic advantage of single-vesicle analysis, we were able to construct a histogram of the rate constants for the first decay, which followed a Poisson distribution, and a histogram of rate constants for the second decay, which was normally distributed. These results suggest two different physical mechanisms for the permeation of protons into a single vesicle over time. We propose that the first decay was due to a transient-pore mechanism and the second to a solubility−diffusion mechanism. In addition, an average permeability coefficient was calculated for the bulk population of vesicles by correlating the decay rate constant and vesicle intensity (dependent on size); however, we found little correlation for individual vesicles, which suggests that proton permeability among single vesicles was heterogeneous in our experiments.

Materials and Methods

Materials. 1-Palmitoyl-2-oleoyl-*sn*-glycero-3-phosphocholine (POPC) was obtained from Avanti Polar Lipids (Alabaster, AL); 5- and 6-carboxyfluorescein were obtained from Molecular Probes (Eugene, OR). Solutions were prepared with deionized water and 50 mM K_2SO_4 (J. T. Baker, Phillipsburg, NJ) and were pH-adjusted with 1 M NaOH and HCl (VWR Scientific, West Chester, PA). We did not use buffer in our system because it competes and interferes with proton binding to carboxyfluorescein; prior to each experiment, we carefully measured and adjusted the pH so that it was consistent across all experiments.

Preparation of Phospholipid Vesicles. Vesicles were prepared at room temperature by extrusion using an Avanti Polar Lipids mini-extruder. Approximately 0.4 g of 25 mg/mL POPC was dried in a glass vial and held under vacuum for >12 h. The lipid was then resuspended and vortexed to form multilamellar vesicles in 1 mL of a solution of 50 mM K_2SO_4 and 10 mM carboxyfluorescein adjusted to pH 9. Vesicles were extruded 19 times through 1-μm pore filters, then 13 times through 400-nm pores, and finally 13 times through 100-nm pores. To increase encapsulation of the fluorescent dye, the extruded vesicles were put through a freeze−thaw cycle in liquid nitrogen and a stream of warm water (∼50 °C). This freeze−thaw cycle led to two populations in vesicle size, one ranging from 70 to 300 nm in diameter and the second ranging from 1 to 10 μm in diameter. Because of the drag force exerted by the flow on the large vesicles in the channel, these larger vesicles did not readily adsorb onto the coverslip, thereby leaving only the small vesicles for subsequent analysis. To remove free dye from the vesicle solution, we used a size-exclusion column (with 3.3 mL of dead volume and a 6-kDa cutoff) from Bio-Rad (Hercules, CA). Experiments were performed within 2 h after the vesicles were prepared.

Microfluidic Channels. Microchannels (200 μm wide, 50 μm tall, 8 cm long) were fabricated in poly(dimethylsiloxane) (PDMS) using rapid prototyping.[23,24] Reservoirs of ∼200-μL volume were punched in the PDMS before oxidation in an oxygen plasma and bonding to a glass coverslip. To facilitate TIRF imaging and to enhance adsorption of the vesicles onto the glass surface, coverslips were boiled in a 3:2:1 water/NH_4OH/H_2O_2 solution for ∼1 h to rid the surface of impurities. Once the PDMS piece had been sealed to the coverslip (48 mm × 65 mm, no. 1 thickness), deionized water was wicked into the oxidized channels to keep the surface hydrated until experiments were performed. Vesicle solution was introduced into the microchannel reservoir and allowed to flow until adequate coverage of the vesicles on the coverslip was obtained. Solution exchange was simple and consisted of removing the solution in the reservoir and replacing it with another solution. After an adequate number of vesicles had adsorbed onto the surface, the solution was changed to 50 mM K_2SO_4 at pH 9 and flowed through the channel to remove free vesicles. To acidify the extravesicular solution, we exchanged solution in the reservoir to 50 mM K_2SO_4 at pH 3.5. Under gravity-driven flow, the proton front traveled at ∼10 mm/s to reach the area where quenching of the fluorescence within single vesicles was viewed. At the imaging area, complete exchange of the solution occurred over a period of ∼5 s.

Total Internal Reflection Fluorescence (TIRF) Microscopy. Measurement of fluorescence quenching in single vesicles was achieved using total internal reflection fluorescence microscopy (Figure 1) and a high-sensitivity CCD camera (Cascade 512B, Roper Scientific, Tucson, AZ). Briefly, 488-nm light from a solid-state diode-pumped laser (Coherent Sapphire, Santa Clara, CA) was focused at the back-focal plane and directed off-axis into a Nikon 100× TIRF objective (NA 1.45). The light was incident at an angle just slightly greater than the critical angle, thus resulting in total internal reflection.[25,26] Fluorescence from the plane of excitation was collected with the objective and passed through a dichroic mirror (z488rdc, Chroma, Rockingham, VT) and filtered by a band-pass filter (HQ550/100M, Chroma, Rockingham, VT) before being imaged by the CCD camera.

(19) Chiu, D. T.; Wilson, C. F.; Karlsson, A.; Danielsson, A.; Lundqvist, A.; Stromberg, A.; Ryttse, F.; Davidson, M.; Nordholm, S.; Orwar, O.; Zare, R. N. *Chem. Phys.* **1999**, *247*, 133.
(20) Sun, B.; Chiu, D. T. *Anal. Chem.* **2005**, *77*, 2770.
(21) Klonis, N.; Sawyer, W. H. *J. Fluoresc.* **1996**, *6*, 147.
(22) Sjoeback, R.; Nygren, J.; Kubista, M. *Spectrochim. Acta A* **1995**, *51A*, L7.
(23) McDonald, J. C.; Whitesides, G. M. *Acc. Chem. Res.* **2002**, *35*, 491.
(24) Fiorini, G. S.; Chiu, D. T. *BioTechniques* **2005**, *38*, 429.
(25) Axelrod, D. *Methods Cell Biol.* **1989**, *30*, 245.
(26) Kuyper, C. L.; Jeffries, G. D. M.; Lorenz, R. M.; Chiu, D. T. In *Nanofabrication Towards Biomedical* Applications; Kumar, C. S. S. R., Hormes, J., Leuschner, C., Eds.; Wiley-VCH: Weinheim, Germany, 2005; p 197.

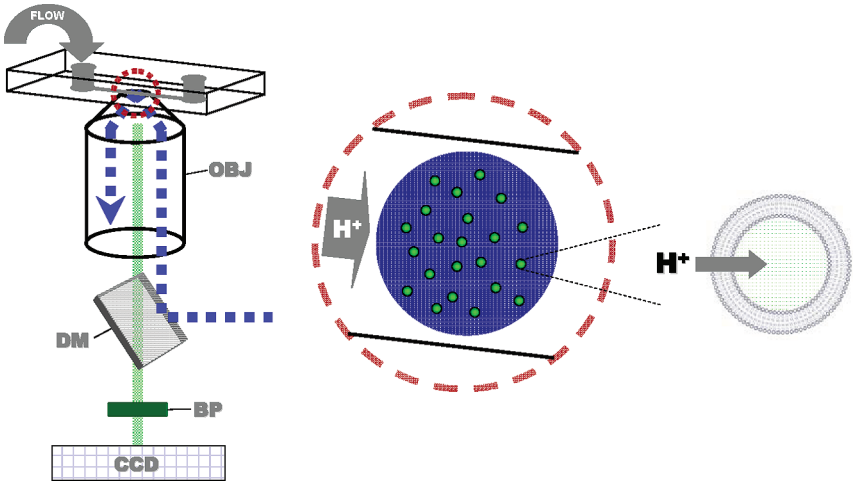

Figure 1. Schematic of the experimental setup. Gravity-driven flow was used to exchange solutions within the microchannel, which was positioned above the high-numerical-aperture (NA of 1.45) objective (OBJ). To achieve total internal reflection fluorescence (TIRF), the 488-nm laser beam was directed from the dichroic mirror (DM) off-axis into the back aperture of the objective, which resulted in an incident angle greater than the critical angle required for total internal reflection. Fluorescence from the vesicles was collected by the objective, sent through a band-pass filter (BP), and then imaged onto a sensitive CCD camera. Vesicles were passed through the microchannel by gravity-driven flow and allowed to adsorb onto the floor (coverslip surface) of the microchannel via nonspecific interactions. Proton-induced quenching of carboxyfluorescein fluorescence occurred once a low-pH solution was exchanged into the microchannel and protons began to enter into the vesicle where carboxyfluorescein was localized.

Rather than using epifluorescence, we used TIRF because it offers higher sensitivity and an increased signal-to-background ratio, which, in turn, permitted us to use lower laser powers to minimize photobleaching. The fluorescence intensity distributions that we recorded with TIRF and epifluorescence showed no discernible differences. Also, as we swelled the 100-nm-diameter vesicles containing carboxyfluorescein, we did not observe any drop in fluorescence intensity, which indicated the presence of a rather thick TIRF illumination depth, as anticipated.

Dynamic Light Scattering. Bulk vesicles were sized using a Brookhaven 90 Plus particle sizer (Holtsville, NY); the accompanying software reported the measured size distribution in a histogram format.

Data Collection. To measure the change in fluorescence intensity over time, we used Metavue 5.1 software (Universal Imaging, Downington, PA) to monitor each individual vesicle in the field of view. Figure 2A shows a representative image. Here, hundreds of individual vesicles were first manually encircled and assigned a number, and then the maximum recorded intensity of each vesicle was plotted over time and transferred into a spreadsheet. Because multilamellar vesicles showed different fluorescence decay profiles than unilamellar vesicles, we separated these two populations by visual analysis of the decay curves, where decays from multilamellar vesicles were recognized by their stepwise quenching profile. For each individual unilamellar vesicle, we recorded the initial intensity and fitted the decay curve to determine the values of rate constants, k_1 and k_2. By analyzing hundreds of single unilamellar vesicles, a histogram of rate constants was generated. During the experiments, some vesicles detached from the glass surface, resulting in an abrupt drop in intensity; these traces were removed from the analysis. Furthermore, we subtracted background intensity from our decay curves, where the background level was obtained by taking the average intensity from the areas that were not illuminated by the laser beam.

Results

Measuring Fluorescence Intensities from Single Vesicles. With an optimized vesicle density on the surface, we were able to record from ~380 vesicles simultaneously within an evenly illuminated imaging area (Figure 2A). Fluorescence recorded from the vesicles arose from dye molecules encapsulated within the vesicle interior. It is possible, however, that some of the observed fluorescence emission could have been derived from dye that adsorbed onto the exterior membrane surface of the vesicles. Dye molecules can attach to membrane surfaces and usually reside at shallow depths near the polar headgroups depending on the hydrophobicity and charge of the molecule.[27] To test for the presence of dyes bound to the exterior membrane surface of the vesicles, we adsorbed POPC vesicles onto the surface of the microchannel. We then flowed through the channel a solution of carboxyfluorescein, followed by a dye-free solution to measure the amount of dye attached to the membrane surface. At the low laser powers (<0.05 W/cm^2) used to monitor proton permeability, we were unable to detect any fluorescence from the vesicles. At higher illumination powers ($\sim$100 W/cm^2), however, we did observe fluorescence from the membrane-bound carboxyfluorescein. Consequently, although a small number of dye molecules might be adsorbed onto the exterior membrane surface, the fluorescence signal we recorded under our experimental conditions arose solely from the encapsulated dye molecules. In addition, because the number of molecules encapsulated within the vesicle volume depended on the starting concentration of carboxyfluorescein before vesicle formation as well as on the number of freeze−thaw cycles used, we held these variables constant for each experiment.

Another potential issue is that, in solution, carboxyfluorescein begins to self-quench between 1 and 2 mM. To ensure that the encapsulated dyes did not self-quench inside the vesicles, we prepared vesicles with starting solution concentrations of 10 and 20 mM carboxyfluorescein, which was necessary because of inefficient encapsulation. After separation from the free external dye, vesicles were adsorbed onto the coverslip, and solution was exchanged in the channel to swell the vesicles osmotically. For the vesicles prepared with 10 mM carboxyfluorescein, we detected no increase in fluorescence as we swelled the vesicles, indicating no self-quenching of the dye inside. In contrast, for the vesicles prepared with 20 mM carboxyfluorescein, we observed increased fluorescence as the swelling occurred,

(27) Kachel, K.; Asuncion-Punzalan, E.; London, E. *Biochim. Biophys. Acta* **1998**, *1374*, 63.

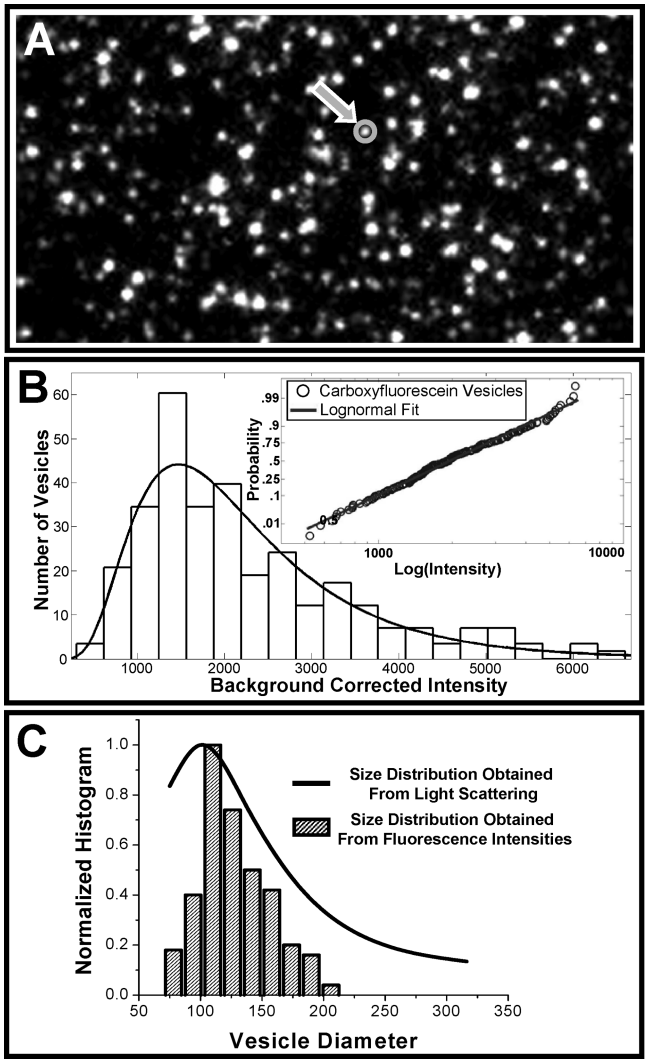

Figure 2. Distribution of fluorescence intensity of single vesicles. (A) Fluorescence image of individual 1-palmitoyl-2-oleoyl-*sn*-glycero-3-phosphocholine (POPC) vesicles, which contained carboxyfluorescein, adsorbed onto the surface of the coverslip. Each vesicle in the image was region-selected, so its maximum intensity would be recorded as a function of time. (B) Histogram that shows the distribution of the background-corrected fluorescence intensity for each vesicle recorded in (A); the histogram fitted well to a log−normal distribution as seen in the log−normal probability plot (inset). (C) Normalized plot that shows the distribution in the diameters of the vesicles. The black line represents measurement using dynamic light scattering; the histogram was plotted by taking the cube root of the fluorescence intensity from each vesicle in B.

because of the decrease in dye concentration as the vesicle volume expanded. A starting concentration of 10 mM carboxyfluorescein, therefore, produced the brightest vesicles and the widest dynamic range for monitoring proton permeability without causing any self-quenching. Through this experiment, we estimated that the carboxyfluorescein concentration inside the vesicles was ≤ 1 mM and that the encapsulation efficiency of dye into the vesicles was significantly less than 100%. In addition, measurements of leakage rates of carboxyfluorescein from POPC vesicles indicated a constant internal concentration over the duration of our experiments. For this measurement, we used a high internal concentration of carboxyfluorescein such that its fluorescence was self-quenched. We then measured the increase in fluorescence intensity over time, which was caused by leakage of dye from the vesicle and a corresponding reduction in self-quenching. This increase in fluorescence intensity was fitted with a single-exponential equation to yield a rate constant, k, of $\sim 4 \times 10^{-5}$ s^{-1}, which was about 3 orders of magnitude lower than k_1 and 2 orders of magnitude lower than k_2. Over the duration of our experiments, therefore, the decrease in fluorescence intensity from dye leakage was negligible.

After collection of the fluorescence intensities from the vesicles, we binned the recorded intensity data into a histogram to show the distribution of intensities for the population of vesicles (Figure 2B). Interestingly, the data were log−normally distributed and could be fitted with a log−normal function, as depicted in the log−normal probability plot (see inset in Figure 2B). This observation agrees with previous studies using cryo-electron microscopy (cryo-EM),[28] atomic force microscopy (AFM),[29] and multi-angle light scattering,[30] which all reported the size of extruded vesicles to exhibit log−normal distributions. Although the mechanism of extrusion is not fully understood, the process has been suggested to involve a random fragmentation pathway where the vesicles are first squeezed into a cylindrical form while passing through the extrusion pores and then broken into smaller structures.[31,32] The log−normal shape of the intensity histogram suggests a correlation between the intensity values and the sizes of the vesicle.

Because the fluorescence intensity from each vesicle is proportional to the volume of the vesicle, we correlated the intensity value with the size of the vesicle. We first independently measured the size distribution of the vesicle population in solution using light scattering, from which we obtained vesicle diameters ranging from 70 to 310 nm (Figure 2C). We then took the cube root of the background-corrected intensity values and binned the values into a histogram (Figure 2C). By comparing this histogram with the size distribution obtained from light scattering, we were able to align the two distributions and correlate the cube root of the background corrected intensity value from each vesicle with the diameter of the vesicle (Figure 2C). The range of vesicle diameters obtained using this method was between $\sim$75 and 210 nm, which was reasonable because unilamellar vesicles are known to rupture and adhere to the glass surface when their diameters exceed $\sim$200 nm.[29,33−37] Moreover, small vesicles tend to adsorb more readily on the glass surface, owing to the drag force exerted by the flow on the vesicles inside the channel.

Proton Quenching of Dye Fluorescence inside Single Unilamellar Vesicles. A number of bulk approaches have been used to study the rates of proton permeability across lipid membranes. Within a closed system and at a high vesicle density, the pH of the extravesicular solution can be measured directly to follow the bulk movement of protons in to and out of the internal vesicle volume.[1] Electrodes also can be used to measure indirectly conductance rates of H^+/OH^- across membranes.[5] Alternatively, spin-labeled probes, which are detected

(28) Egelhaaf, S. U.; Wehrli, E.; Muller, M.; Adrian, M.; Schurtenberger, P. *J. Microsc.* **1996**, *184*, 214.
(29) Reviakine, I.; Brisson, A. *Langmuir* **2000**, *16*, 1806.
(30) Korgel, B. A.; van Zanten, J. H.; Monbouquette, H. G. *Biophys. J.* **1998**, *74*, 3264.
(31) Tenchov, B. G.; Yanev, T. K. *J. Colloid Interface Sci.* **1986**, *111*, 1.
(32) Clerc, S. G.; Thompson, T. E. *Biophys. J.* **1994**, *67*, 475.
(33) Seifert, U.; Lipowsky, R. *Phys. Rev. A: Atomic, Molec., Opt. Phys.* **1990**, *42*, 4768.
(34) Nollert, P.; Kiefer, H.; Jahnig, F. *Biophys. J.* **1995**, *69*, 1447.
(35) Keller, C. A.; Kasemo, B. *Biophys. J.* **1998**, *75*, 1397.
(36) Egawa, H.; Furusawa, K. *Langmuir* **1999**, *15*, 1660.
(37) Johnson, J. M.; Ha, T.; Chu, S.; Boxer, S. G. *Biophys. J.* **2002**, *83*, 3371.

by electroparamagnetic resonance and sensitive to transmembrane potentials, can be used to monitor the transport of protons across the membrane indirectly.[3] Although these methods work for bulk measurements, single-vesicle studies require sensitive detection, which most often relies on fluorescence sensing. Here, we encapsulated the pH-sensitive probe carboxyfluorescein inside the vesicles to visualize directly the transit of protons into the vesicle as the pH outside the vesicle was lowered. Conveniently, many bulk studies have also used this approach, so we can compare our single-vesicle data with bulk measurements.

Several bulk pH-jump experiments reported a biphasic decay in the fluorescence of a pH-sensitive dye that was encapsulated within a vesicle.[9,38,39] To explain this biphasic decay, Clement and Gould hypothesized that the first decay was caused by the dissipation of an electrical potential across the membrane.[38] Once the potential had been dissipated, they suggested, proton permeation continued to be driven by a concentration gradient but was hindered by the effusion of positive ions out of the vesicle to maintain charge neutrality. Deamer and co-workers suggested two exponential decays because, for pyranine, fluorescence was not a linear function of pH.[39] The mechanistic origin of this biphasic decay is not well understood, and from bulk methods, it is unclear whether multiple decays originated from different populations of vesicles that existed in the sample. With single-vesicle analysis, we hope to gain a better understanding of proton diffusion across the lipid bilayer.

The general procedure of our experiments was first to image the starting intensities of single vesicles and then to exchange the solution in the microchannel from high pH (9.0) to low pH (3.5). As a control experiment, we measured the fluorescence intensity from the vesicles over a typical experimental runtime (5 min) without any pH drop. Owing to the poor photostability of carboxyfluorescein and our long observation time, photobleaching was an issue. To overcome bleaching, we had to use very low laser excitation power densities ($\sim$0.03 W/cm^2), which rendered photobleaching minimal ($<$10% over 5 min) under our experimental conditions. We also verified that photobleaching of fluorescein was relatively pH-independent. The compromise with using such a low power density is the need to use relatively long integration times (1 s) for each data point. Because the channel was under a constant slow flow, we assumed that the external proton concentration remained constant during our experiments (at pH 3.5) and that the final pH inside the vesicle would eventually reach 3.5. At the low laser excitation intensities used in our experiment, this pH will result in zero fluorescence from the vesicle. Indeed, we imaged vesicles after 1 h of exposure to an external solution of pH 3.5 and detected no fluorescence from the vesicles.

Figure 3A shows the fluorescence quenching profile averaged over $\sim$190 vesicles as the pH in the microchannel was lowered from 9.0 to 3.5. For carboxyfluorescein, fluorescence intensity is linearly proportional to pH within the range of 9−5. Over the duration of our experiments, the pH inside the vesicles did not drop below 5. Therefore, we assumed a linear relationship between the intravesicular pH drop and the fluorescence intensity decay. This quenching profile shows clearly the

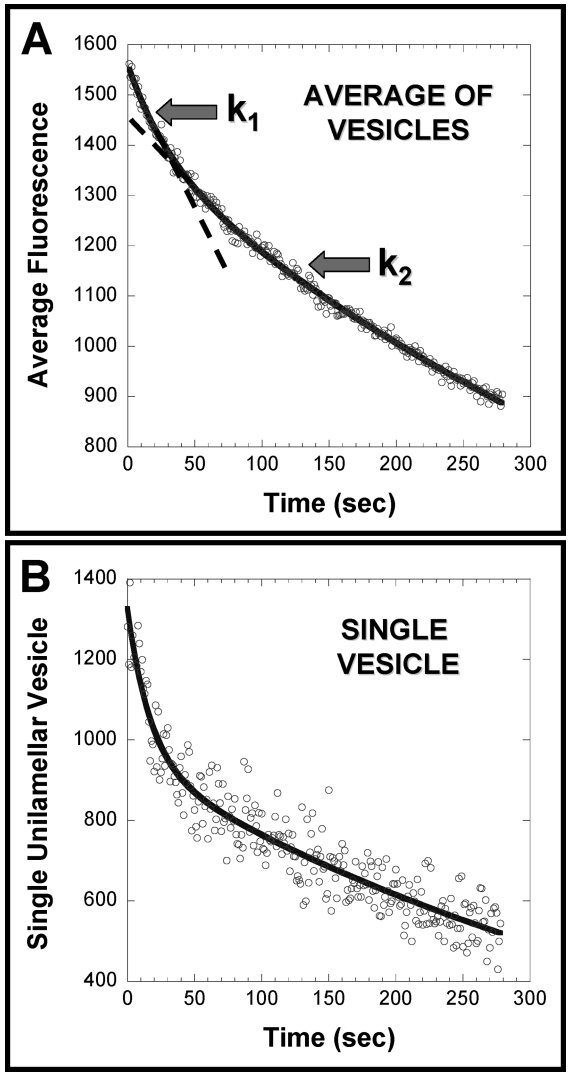

Figure 3. Fluorescence quenching profile of unilamellar vesicles. (A) Averaged quenching profile obtained from $\sim$190 single-vesicle traces, which was fitted to obtain a mean value of 0.032 s^{-1} for k_1 and 0.0016 s^{-1} for k_2. (B) Single-vesicle fluorescence-quenching curve, which had values of $k_1 = 0.068 \pm 0.009$ s^{-1} and $k_2 = 0.0015 \pm 0.0006$ s^{-1}.

presence of two exponential decays, which we fitted using the equation

$$F(t) \propto [\mathrm{C}^*](t) = [\mathrm{C}^*]_{\mathrm{initial}} - \{[\mathrm{H}^+]_1(1 - \exp^{-k_1 t}) + [\mathrm{H}^+]_2(1 - \exp^{-k_2 t})\} \quad (1)$$

where $F(t)$ and $[\mathrm{C}^*](t)$ are the fluorescence and concentration of carboxyfluorescein, respectively, as functions of time; $[\mathrm{C}^*]_{\mathrm{initial}}$ is the initial concentration of carboxyfluorescein; $[\mathrm{H}^+]_1$ and $[\mathrm{H}^+]_2$ are the concentrations of protons that entered during the first and second exponential decays, respectively; and k_1 and k_2 are the respective rate constants for the two exponential decays.

Permeability of ions can be estimated with the equation

$$P_{\mathrm{ion}} = k\left(\frac{R_{\mathrm{vesicle}}}{3}\right) \quad (2)$$

where the permeability coefficient of the ion, P_{ion}, is related to R_{vesicle}, the radius of the individual vesicles, and k is the exponential rate constant (obtained from eq 1). Figure 3A shows

(38) Clement, N. R.; Gould, J. M. *Biochemistry* **1981**, *20*, 1534.
(39) Paula, S.; Volkov, A. G.; Van Hoek, A. N.; Haines, T. H.; Deamer, D. W. *Biophys. J.* **1996**, *70*, 339.

the population-averaged decay trace for ~190 unilamellar vesicles, which were fitted with eq 1 to obtain values of 0.032 s^{-1} for the first rate constant (k_1) and 0.0016 s^{-1} for the second rate constant (k_2).

Using these rate constants and an average vesicle radius of 65 nm (obtained from light-scattering measurements), we used eq 2 to calculate permeability coefficients of 2×10^{-7} cm/s for the first phase of the decay and 1×10^{-8} cm/s for the second decay phase. The permeability coefficient of 2×10^{-7} cm/s obtained for the first exponential decay agrees with published values of proton permeability into POPC vesicles, which are on the order of 10^{-7} cm/s.[8] The second permeability coefficient of 1×10^{-8} cm/s was significantly lower than the first; on the basis of observations by Clement and Gould,[38] we believe that this second permeability constant corresponds to the rate of K^+ permeation. Upon addition of valinomycin, a molecule that binds to K^+ ions and increases the permeability of K^+ across the membrane, the rate of the second decay was dramatically increased, thus further suggesting that K^+ ions control the permeability in this regime.[39,40] Published values of K^+ permeability across membranes range from 10^{-9} to 10^{-13} cm/s. The faster K^+ permeability of 10^{-8} cm/s in our experiments might be caused by the strain and higher tension exerted on the membrane as the vesicle adsorbed onto the glass surface. In addition, for vesicles comprising only 1,2-dioleoyloxy-3-trimethylammonium propane (DOTAP), k_1 was ~180 times higher than k_2, which was notable in comparison to POPC vesicles (where k_1 was ~20 times higher than k_2). DOTAP vesicles are less stable than POPC vesicles; this difference in stability might have caused the difference in the k_1/k_2 ratio. Also, we observed roughly a linear correlation between the vesicle volume and the k_1/k_2 ratio, suggesting that this ratio of rates might be related to the stability of the lipid membrane.

Figure 3B shows a decay curve obtained for a single vesicle. Here, the vesicle lost 25−30% of its fluorescence during the first phase of the decay, with a corresponding rate constant (k_1) of 0.068 ± 0.009 s^{-1}. After this initial phase of fast proton permeation into the vesicle, the permeability slowed by a factor of 45, i.e., the rate constant decreased to 0.0015 ± 0.0006 s^{-1}, in the second phase (k_2). From our single-vesicle measurements, we observe that proton permeation into lipid vesicles occurs via a sequential two-step mechanism, an initial fast phase followed by a slower second phase, which is likely rate limited by the efflux of K^+ from the vesicle.

Proton Permeation into Single Multilamellar Vesicles. The strength of single-vesicle analysis lies in the ability to visualize individual events that would otherwise be masked in population-averaged measurements. The observation that proton permeation into vesicles occurs via a two-step process provides one example. Another example is the ability to "see" rare events, which, in our case, is the sequential permeation of protons across lipid membranes of multilamellar vesicles. For extruded vesicles, the percentage of multilamellar vesicles present depends on the average size of the vesicles. Cullis and co-workers used ^{31}P-quenching NMR to calculate these percentages and found them to increase from 0% to ~20% as the average diameters of the vesicles increased from 100 to 200 nm.[17] Because we could "watch" proton permeation into each vesicle, we could directly ascertain the percentage of multilamellar vesicles present in our sample. Of the 380 vesicles analyzed in our experiment, 42 vesicles were multilamellar, which represented ~11% of the vesicle population. Furthermore, we observed the percentage of multilamellar vesicles to increase with the size of the vesicles, that is, with vesicles that showed higher fluorescence intensities.

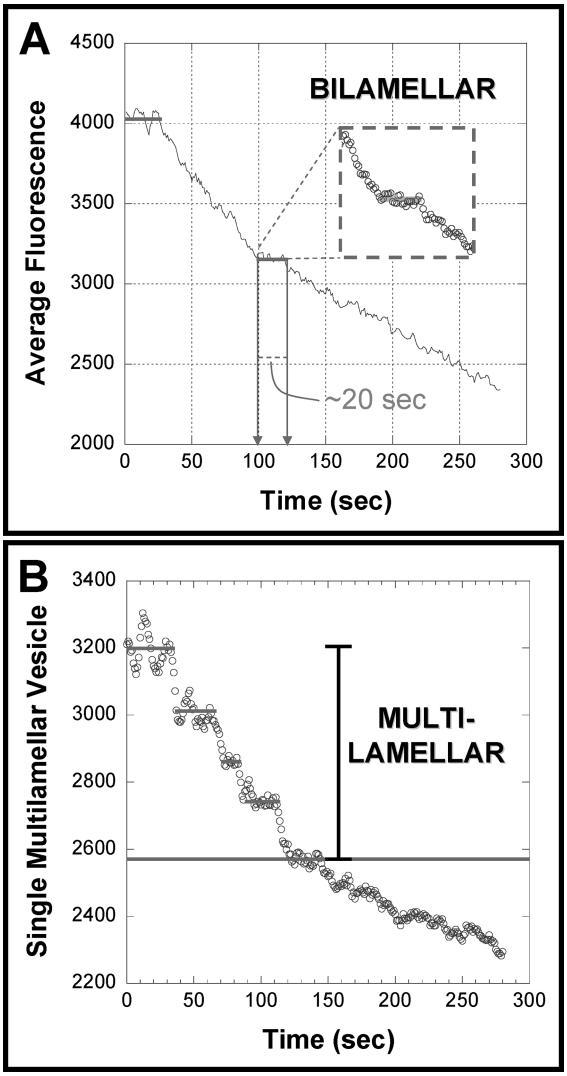

Figure 4. Fluorescence quenching profile of multilamellar vesicles. (A) Averaged quenching curve from ~35 bilamellar vesicles showing two plateaus (inset shows one plateau) that lasted ~20s and were due to a reduced rate of quenching. (B) Quenching curve of a multilamellar vesicle, which had five plateaus lasting ~10−30 s.

Figure 4A shows a population-averaged decay trace for ~35 bilamellar vesicles, and Figure 4B shows the trace for a single multilamellar vesicle. In contrast to the trace for unilamellar vesicles (Figure 3B), multilamellar vesicles showed plateaus or steps in the fluorescence decay profile; these steps, which last tens of seconds, were estimated by visual analysis. For bilamellar vesicles (Figure 4A), two plateaus (inset shows one plateau) were present, each lasting on average ~20s . Vesicles that contained more than two lipid membranes were rarer. Figure 4B shows one example, in which the vesicle contained five lamellae. Proton permeation through the lamellae lasted ~10−30 s, a duration similar to that observed for the bilamellar vesicles (Figure 4A). Each drop corresponded to the complete quenching of carboxyfluorescein in the interlamellar space before permeation of accumulated protons across the next layer of the lipid membrane, which formed the plateau. The variability

(40) Papahadjopoulos, D. *Biochim. Biophys. Acta* **1971**, *241*, 254.

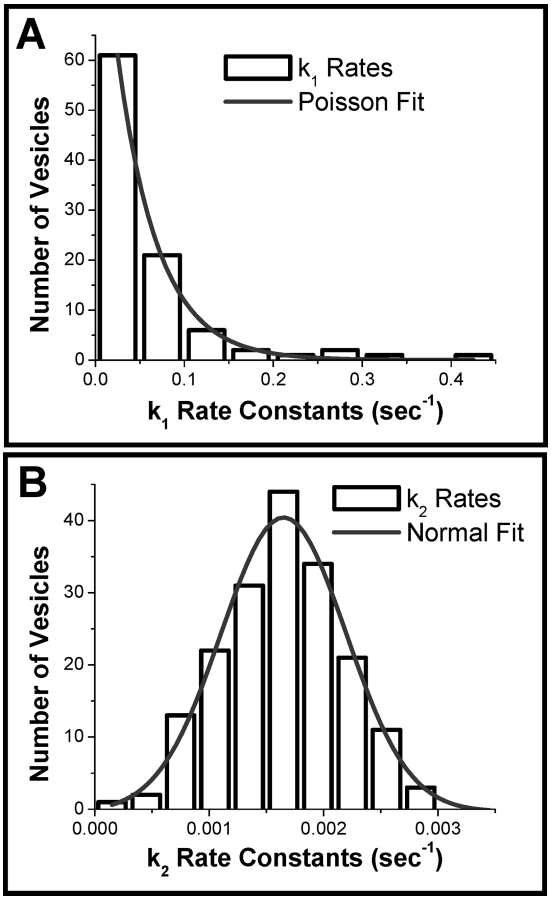

Figure 5. Distribution of permeability rate constants. (A) Histogram showing that the distribution of k_1 fits a Poisson distribution with high correlation ($R^2 = 0.96$). (B) Histogram showing that k_2 is normally distributed ($R^2 = 0.99$).

in the length of time for each plateau might have been caused by differences in the number of dye molecules present in the interlamellar volume, as well as by heterogeneity among the rates of diffusion across each membrane layer.

Discussion

Distributions of Proton Permeability Rates for Single Unilamellar Vesicles. Bulk vesicle studies provide information about averaged values, but single-vesicle analysis offers additional information on the distribution about the mean value. Figure 5 shows the histograms of the two rate constants, k_1 and k_2, for each phase of proton permeation into the vesicles. To generate the histograms, each single-vesicle trace was first fitted to obtain the rate constants of each phase (Figure 3B) of the fluorescence decay profile. Second, the rate constants were then binned against the number of vesicles that exhibited a particular value. Figure 5A shows the distribution for the first rate constant (k_1), which follows a Poisson distribution ($R^2 = 0.96$). In contrast, the second rate constant (k_2) was normally distributed ($R^2 = 0.99$) (Figure 5B). The two distinct distributions exhibited by the rate constants, k_1 and k_2, suggest that very different physical mechanisms underlie the two phases of proton permeation into the vesicles.

Two models of ion permeability through membranes have been proposed: (1) the transient-pore model and (2) the solubility−diffusion model.[10] The transient-pore model suggests that ions flow across the membrane en masse through pores that randomly form in the membrane. Hamilton and Kaler described this mechanism for movement of alkali metals across thin lipid bilayers,[41] whereas Deamer and co-workers showed that the prevalence of pore formation depended on the thickness of the bilayer membrane.[39] In contrast, the solubility−diffusion model stems from early studies by Overton[42] and states that ions in solution first partition into the outer leaflet of the membrane, then diffuse through the hydrophobic core of the lipid tails, and finally partition out of the inner leaflet of the bilayer and into the solution on the other side of the membrane.[10,43]

A Poisson distribution indicates that the first decay rate constants were dependent upon a rare, random process such as formation of a small number of transient pores or defects. The majority of the vesicles exhibited rate constants of $<0.05\ s^{-1}$; however, vesicle permeabilities ranged out to 6 times that value. Pore formation in our experiments was likely caused by the presence of both osmotic and electrical potential gradients established across the vesicle membrane as the extravesicular solution was exchanged from a 50 mM K_2SO_4 solution at pH 9 to 50 mM K_2SO_4 at pH 3.5. Because the external pH 3.5 solution did not contain carboxyfluorescein, the vesicles could swell slightly under this osmotic pressure. In addition, an electrical potential was produced across the membrane because of ion concentration imbalances between the internal and external solutions. Therefore, both the osmotic and electrical gradients could have acted to destabilize the membrane, thus promoting pore formation during the first decay (k_1) of proton permeation into the vesicles until both gradients came close to equilibration near the end of the first phase.

The normal distribution displayed by the second phase (k_2) of proton permeation into the vesicles was consistent with the solubility−diffusion model, which is independent of pore formation and, in our case, was related to the diffusion of potassium ions through the membrane. This second phase was driven by the concentration gradient of H^+ across the membrane. Because electroneutrality must be maintained across the membrane, for each H^+ ion that entered the vesicle, another positive ion (which is K^+ in our experiments) must exit the vesicle. Consequently, the rate-limiting step during this second phase was the efflux of K^+ from the vesicle, rather than the permeation of H^+ into the vesicle. The rate constant for this second phase (k_2) varied widely, with a large coefficient of variation (CV) of ~88%.

Permeability Coefficients are Heterogeneous Among Single Vesicles. Because the permeability coefficient (P_{ion}) is related to the exponential rate constant (k) and the radius of the vesicles ($R_{vesicle}$) (see eq 2), we could correlate the distribution of k_2 with the distribution in size measured for the vesicles. If the permeability coefficients among the vesicles were homogeneous, then a plot of k_2 vs $R_{vesicle}$ would result in a straight line having a slope of P_{ion}^{-1} (eq 2). Figure 6 presents such a plot; rather than falling on a straight line, the plotted points are highly scattered. The variability in k_2 was not correlated with $R_{vesicle}$. The presence of a single peak in the landscape plot of Figure 6B, however, is consistent with eq 2 and correlates well with bulk studies, which are able to relate only the average value of k_2 to the average value of $R_{vesicle}$.

(41) Hamilton, R. T.; Kaler, E. W. *J. Phys. Chem.* **1990**, *94*, 2560.
(42) Overton, E. *Vierteljahreschr. Naturforsch. Ges. (Zürich)* **1899**, *44*, 88.
(43) Al-Awqati, Q. *Nat. Cell Biol.* **1999**, *1*, E201.

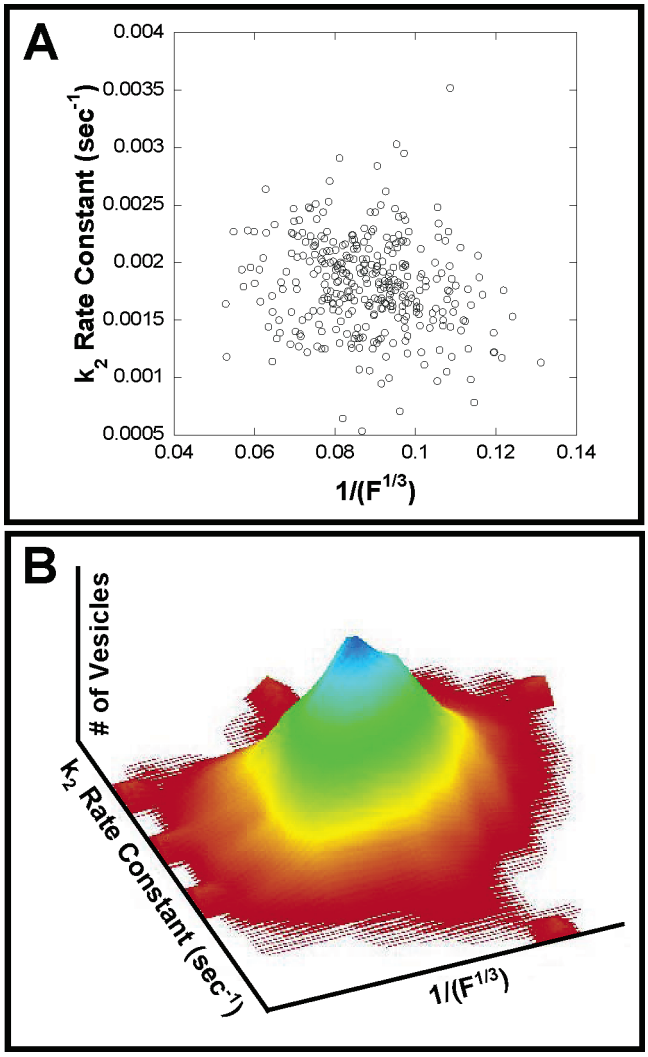

Figure 6. Plots of k_2 against the inverse of the cube root of fluorescence intensity ($1/F^{1/3}$) (which is proportional to the radius of the vesicle) of single vesicles in (A) scatter and (B) landscape format.

In its simplest form (for the solubility−diffusion model), the flux of protons into the vesicle can be described by the equation

$$J_{H^+} = \frac{d(V_{vesicle}[H^+]_{in})}{dt} = \frac{K_{H^+}D_{H^+}}{l_{membrane}}([H^+]_{out} - [H^+]_{in})(A_{vesicle})(B_{vesicle}) \quad (3)$$

where J_{H^+} is the flux of protons per second; $V_{vesicle}$ is the internal volume of the vesicle; $A_{vesicle}$ is the surface area of the vesicle; $B_{vesicle}$ is the buffering capacity, or the number of molecules within the vesicle that can bind to a proton; K_{H^+} is the partitioning coefficient of the proton into the membrane; D_{H^+} is the diffusion coefficient of protons within the membrane; $l_{membrane}$ is the thickness of the membrane; and $[H^+]_{out}$ and $[H^+]_{in}$ are the proton concentrations inside and outside the vesicle, respectively. The observation of high degrees of variability in k_2 from the single-vesicle measurements suggests that each vesicle likely exhibits slightly different partitioning (K_{H^+}) and diffusion (D_{H^+}) coefficients and membrane thicknesses ($l_{membrane}$), which might be caused by differences in the local physical and chemical environment.

Conclusions

With advances in sensitive detection and the ability to monitor the chemical changes that occur in ultrasmall volumes, single-vesicle studies offer a new avenue toward gaining a better understanding about biologically relevant processes. Using this approach, we found proton permeability across membranes to occur through a sequential two-step mechanism, starting with a transient-pore phase followed by a diffusion-limited exchange of extravesicular protons with intravesicular positive ions (K^+ in this case). This new mechanistic detail was made possible by the ability to follow proton permeation into a single vesicle, as well as by the additional information on the statistical distribution about the mean rate of proton permeability. The Poisson distribution obtained during the initial phase of proton permeation implicates a transient-pore mechanism, and the normal distribution observed for the later phase is consistent with a solubility−diffusion model. As anticipated from bulk measurements, we observed a correlation between the average vesicle size and the average rate constant for proton permeation. At the single-vesicle level, however, we found little correlation between the observed rate of proton permeation and the size of each vesicle. This finding suggests that proton permeability is heterogeneous among the vesicles, which might be caused by slight differences in the local chemical and physical environment experienced by each vesicle. We anticipate single-vesicle studies to provide other important information that is otherwise buried in bulk analysis.

Acknowledgment. C.L.K. gratefully acknowledges support from the NSF for a graduate research fellowship. We thank Professor John A. Glomset for the use of the dynamic light-scattering system for vesicle sizing. Funding of this work was provided by the National Institutes of Health (R01 GM65293).

JA057349C